JOURNAL OF GEOPHYSICAL RESEARCH, VOL. 115, D14203, doi:10.1029/2009JD013143, 2010

Vertical distributions of lightning sources and flashes over Kennedy Space Center, Florida

Amanda E. Hansen,[1] Henry E. Fuelberg,[1] and Kenneth E. Pickering[2]

Received 3 September 2009; revised 24 February 2010; accepted 5 March 2010; published 21 July 2010.

[1] Warm season vertical distributions of lightning sources and flash segments are presented using data from the lightning detection and ranging network at Kennedy Space Center, Fla. We emphasize the percentage of sources/flash segments at each level compared to the vertical total and present the distributions as a function of storm top above ground level (AGL). The vertical profiles of sources and flash segments are compared with each other and with those from previous studies. Results indicate that storms with tops higher than ~10 km AGL often have a bimodal or multiple peak distribution of percentage sources and flash segments. However, distributions for storms with tops lower than ~10 km AGL exhibit only a single dominant peak. Temporal variations in the vertical distributions of flash percentages are examined for four clusters of storms occurring on different days. Results reveal considerable storm-to-storm and intrastorm variability. However, two similarities are observed between the four cases: (1) maximum flash density (flash segments km^{-3}) occurs as the maximum storm top is reached and (2) as the storms increase in intensity, both maximum flash density and flash segment percentage increase in altitude, and then both decrease in altitude as the storms decay. The distributions are useful for understanding lightning characteristics as a function of storm evolution, specifying the vertical distribution of lightning-produced nitrogen oxides in chemical transport models and verifying model-simulated lightning.

Citation: Hansen, A. E., H. E. Fuelberg, and K. E. Pickering (2010), Vertical distributions of lightning sources and flashes over Kennedy Space Center, Florida, *J. Geophys. Res.*, *115*, D14203, doi:10.1029/2009JD013143.

1. Introduction

[2] A knowledge of the occurrence and 3-D distribution of lightning is important to many disciplines. Cloud-to-ground (CG) lightning is the second leading cause of weather-related fatalities in the United States, with the National Lightning Safety Institute estimating that lightning causes an annual economic impact of $4–$6 billion [*Curran et al.*, 2000]. Lightning strikes impact transportation, electrical, and communication systems and are the leading cause of wild fires which impact the carbon cycle [*Stocks et al.*, 2002]. Lightning also is an important source of nitrogen oxides (NOx) in the middle and upper troposphere that play a direct role in producing tropospheric ozone [e.g., *Pickering et al.*, 1998; *DeCaria et al.*, 2005, *Ott et al.*, 2007; *Schumann and Huntrieser*, 2007].

[3] Advancements in ground-based lightning detection have improved our ability to explore relationships between lightning and thunderstorm characteristics. These advancements include deployments of the National Lightning Detection Network (NLDN) [*Orville*, 2008] and the lightning detection and ranging (LDAR) [e.g., *Lennon*, 1975; *Poehler and Lennon*, 1979] and lightning mapping array (LMA) [e.g., *Rison et al.*, 1999] networks that have been installed in several regions across North America. The NLDN mostly detects CG flashes, while the LDAR and LMA networks can locate in three dimensions the individual impulsive VHF radiation sources emitted by both CG and intracloud (IC) lightning.

[4] A number of studies have investigated the vertical distribution of VHF lightning sources using the LDAR/LMA networks. However, most have focused on severe convection [e.g., *Krehbiel et al.*, 2000; *Lyons et al.*, 2003; *Carey et al.*, 2005; *Dotzek et al.*, 2005; *Goodman et al.*, 2005; *Ely et al.*, 2008; *Hodapp et al.*, 2008; *Lang and Rutledge*, 2008]. For example, *Carey et al.* [2005] examined the 3-D distribution of VHF sources associated with CG strikes in a mature leading line trailing stratiform (LLTS) mesoscale convective system (MCS). They found fewer VHF sources within the stratiform region compared to the convective region and source densities that decreased with increasing distance rearward of the convective line. They showed that the great majority of VHF lightning sources occurred within the leading convective line and in a bimodal vertical distribution, with one peak near 4.5 km AGL (above ground level) and the other near 9.5 km AGL. *Carey et al.* [2005] and *Hodapp et al.* [2008] showed that the layer of maximum total lightning in their MCS studies

[1]Department of Meteorology, Florida State University, Tallahassee, Florida, USA.
[2]NASA Goddard Space Flight Center, Greenbelt, Maryland, USA.

0148-0227/10/2009JD013143

sloped rearward and downward from the convective region to the stratiform region. *Ely et al.* [2008] examined the 3-D structure of lightning sources within a LLTS MCS near Houston, Tex, focusing on the evolution of precipitation and lightning structure.

[5] *Bruning et al.* [2007] recently examined a multicellular nonsevere storm during the thunderstorm electrification and lightning experiment field program. Although the major purpose was to relate charging and lightning to a storm's convective motions, they also presented vertical profiles of sources occurring in a nonsevere thunderstorm that occurred near Oklahoma City. Results showed that most sources occurred in the storm's positive charge region between 6 and 8 km; however, early on, there was a significant and active lower positive charge center at 4 km. Although a traditional tripole has a less significant lower positive charge region, numerical simulations have indicated that noninductive (NI) charge separation at higher altitudes can enhance the main negative charge [*Mansell et al.*, 2010]. The result is a tripole charge structure with a more significant positive charge region at lower levels than higher levels. *Bruning et al.* [2007] also noted negative charge regions between 4.5 to 6 km and near 8.5 km. The negative charge layer at 8.5 km had few to no associated sources and probably was a screening layer not due to NI charging.

[6] There is increasing interest in modeling lightning and its chemical byproduct NOx [e.g., *Price and Rind*, 1992; *Pickering et al.*, 1998; *DeCaria et al.*, 2005; *Barthe et al.*, 2007; *Barthe and Barth*, 2008; *Ott et al.*, 2007, 2010]. Lightning NOx can efficiently catalyze ozone production in the upper troposphere where ozone is most effective as a greenhouse gas. Therefore, it is important to understand the vertical distribution of lightning. A relation between radar reflectivity and lightning flash rate was derived by *Futyan and Del Genio* [2007] for use in global chemical transport models. Using Tropical Rainfall Measuring Mission satellite observations from the lightning imaging sensor and precipitation radar sensors, they studied over 1500 storms in the region of Africa and the Atlantic Ocean. They found an approximately fifth-order relationship between storm top and flash rate and a second-order relationship between storm height above freezing level and flash rate. The second-order fit provided slightly better results.

[7] Expanding on the results of *Futyan and Del Genio* [2007], this paper explores the relation between radar reflectivity, radar-derived storm top height above freezing level, and the vertical distribution of lightning sources and flash segments. Specifically, our objective is to determine the vertical distribution of flash segments comprising IC and CG (i.e., total) lightning detected by the Kennedy Space Center LDAR network. We emphasize vertical profiles of the percentage of sources and flash segments to distinguish our results from those of previous studies. The vertical distributions of flash segments will be useful in chemical transport models that are run at the regional scale (~10–12 km) to vertically distribute the NOx formed by lightning, as well as to verify model-simulated lightning. We investigate storms of all intensities during a 3 month period (June, July, and August) in 2004 and 2005 when lightning is most common in Florida. The vertical lightning source and flash distributions are related to radar-derived storm heights (specifically height above freezing level) and to radar reflectivity. We first analyze VHF source and flash segment frequencies for the entire summer periods of the 2 years and then expand the discussion to four multicellular storms.

2. Data and Methodology

[8] Data from the Kennedy Space Center LDAR network were used in conjunction with WSR-88D radar data from the nearby Melbourne, Fla, National Weather Service Office (KMLB) to determine the relationship between radar-derived echo top and lightning. This section describes the radar data, domain selection, our procedure for determining radar derived storm top, and the lightning data.

2.1. Weather Surveillance Radar 88 Doppler (WSR-88D) and Domain Selection

[9] The Melbourne, Fla (KMLB) WSR-88D is an operational National Weather Service Doppler radar [*Crum and Alberty*, 1993] located approximately 50 km south of the LDAR central receiver. Level II radar data for KMLB were obtained from the National Climatic Data Center. During times of precipitation, the WSR-88D operates in either of two volume coverage patterns (VCPs), VCP-21 and VCP-11, depending on storm intensity. A VCP-21 scan consists of data at nine elevation angles (0.5°, 1.45°, 2.4°, 3.35°, 4.3°, 6.0°, 9.9°, 14.6°, and 19.5°), while a VCP-11 scan consists of fourteen elevation angles (0.5°, 1.45°, 2.4°, 3.35°, 4.3°, 5.25°, 6.2°, 7.5°, 8.7°, 10.0°, 12.0°, 14.0°, 16.7°, and 19.5°). We used data from both VCPs without differentiation.

[10] We restricted our domain to the area north of the KSC LDAR site since the KMLB VCPs provide incomplete vertical coverage of storm tops south of the LDAR. Specifically, our domain is the northern half of the 50 km radius around the LDAR central receiver. The highest elevation radar beam in this area is at least 17 km above ground based on standard atmospheric conditions. Few storm heights in the area exceed this altitude.

[11] WSR-88D reflectivity data contain both meteorological and nonmeteorological events. Radar contamination can arise from anomalous propagation, ground clutter, bright banding, and clear-air returns. Therefore, we quality controlled the data using the Warning Decision Support System-Integrated Information (WDSS-II) software [*Lakshmanan et al.*, 2007b] that was developed at the National Severe Storms Laboratory and the Cooperative Institute for Mesoscale Meteorological Studies at the University of Oklahoma. *Lakshmanan et al.* [2007a] describe how WDSS-II quality controls radar reflectivity. The resulting quality controlled reflectivity output from WDSS-II was transformed from radar to Cartesian coordinates with a horizontal grid spacing of 1 km and a vertical grid spacing of 0.25 km. The gridded data then were used to determine echo top (maximum height of the 18.5 dBZ contour) at each grid point. This threshold is similar to that used in the WSR-88D radar algorithm to determine tops [*U.S. Department of Commerce*, 2006; *Amburn and Wolf*, 1997]. Mean reflectivity, used later in Figures 5–8a and 8b, was calculated by first converting from logarithmic units (dBZ) to linear units ($mm^6\ m^{-3}$), averaging over grid points that

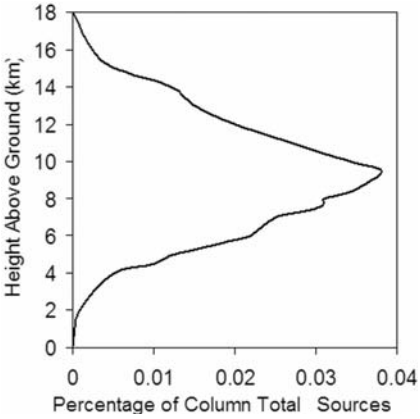

Figure 1. Vertical distribution of mean VHF source densities within 50 km of the KSC LDAR network during a 19 month period from 1997–1998. (After *Boccippio et al.* [2000]).

contained a reflectivity value and then converting the mean back to logarithmic units (dBZ).

2.2. Lightning Detection and Ranging (LDAR) Network

[12] We used lightning data from the LDAR network developed at NASA Kennedy Space Center (KSC) [*Lennon*, 1975; *Poehler and Lennon*, 1979; *Maier et al.*, 1995; *Britt et al.*, 1998; *Boccippio et al.*, 2000]. LDAR uses time of arrival measurements to locate in three dimensions the impulsive VHF radiation emitted by lightning at a frequency of 66 MHz and a bandwidth of 6 MHz [*McNamara*, 2002]. The VHF electromagnetic pulses generated by the individual stepped leaders of each lightning flash are referred to as "sources" or "sparks." LDAR detects sources from IC flashes and the upper portions of CG flashes, with negative leaders being preferentially detected [*Shao and Krehbiel*, 1996] since sources associated with negative breakdown radiate greater power [*Thomas et al.*, 2001]. LDAR has reduced detection efficiency below 2 km altitude and does not detect and locate events that occur during long continuous radiation (such as return strokes). As a result, we can expect some error below 2 km in our vertical distributions.

[13] The KSC LDAR has a typical detection range of 100 km [*Boccippio et al.*, 2000], and according to the Applied Meteorology Unit, has a detection efficiency of approximately 97% within that range, increasing to 99% when events occur within 25 km of the central receiver [*Maier et al.*, 1995; *Murphy et al.*, 2000]. Although improvements to the network during 2007 increased the range of large detection efficiencies (W. Roeder, personal communication, 2009), our period of study is before these upgrades were completed.

[14] *Boccippio et al.* [2000] showed that some KSC LDAR sources were located at "spurious" altitudes above 18 km AGL but that the vertical distributions were stable within 50 km of the LDAR. We only examine lightning sources within the northern 50 km radius of the central receiver site located at 28°32′18.22″ latitude and 80°38″ 33.48′ longitude and altitudes up to 18 km. Lightning from all storms, regardless of their intensity, are considered.

2.3. Flash Creation Methodology

[15] We grouped the VHF lightning source data into 6 min intervals that matched the volume scan periods of the KMLB radar. The individual source data then were combined into flashes using temporal and spatial constraints following the study of *Nelson* [2002]. For a source to be included in a flash, it had to occur within 3 s of the first observed source. Furthermore, each source had to be within 0.5 s of the previous source comprising a flash. This process takes into account LDAR's location and azimuth errors, as described by *Nelson* [2002]. One should note that each of the created flashes could consist of multiple segments or branches of varying lengths. In creating the vertical flash profiles shown in section 3, we considered all segments of each flash, regardless of their length. The source and flash data then were placed onto a 1 × 1 km horizontal grid with 0.25 km vertical spacing up to 18 km, thereby, agreeing with the grid used for the radar data. The gridded data were used to calculate source and flash densities (sources or flash segments km^{-3}) by summing all sources/flash segments within our domain and then dividing by the volume of the domain that contained grid cells with at least one source or flash segment. This allowed comparisons between different storm days. Source and flash percentage were calculated by dividing the number of sources or flash segments in each 0.25 km layer by the vertical sum of all sources or flash segments.

2.4. Atmospheric Sounding Data

[16] Radiosonde soundings from KSC were used to determine freezing level heights over the area. However, we found that during June, July, and August, the freezing level exhibited almost no day-to-day variation, remaining at ~4.5 km. Therefore, we assumed this altitude on all study days that allowed height above the freezing level to be easily converted into height above ground level (AGL) that is used in the results that follow.

3. Results

3.1. Summertime Mean

[17] Except for *Boccippio et al.* [2000] and Buechler (Personal communication, 2009), few studies have examined climatological aspects of the vertical distribution of lightning sources. We first present their results as background before comparing with those of our current study.

[18] *Boccippio et al.* [2000] presented vertical distributions of source densities for all storms near KSC during a 19 month period from March 1997 to September 1998 (Figure 1). Their distribution of source densities within a 50 km radius of the KSC LDAR central receiver exhibits a single maximum at ~9.5 km altitude. Buechler's warm season distribution of VHF source frequencies within 50 km of the North Alabama central LMA receiver (Figure 2) is similar to the annual distribution by *Boccippio et al.* [2000] for central Florida in that both exhibit distinct maxima near 9–10 km. However, the North Alabama warm season distribution also has a secondary peak near 5 km that is not observed at KSC. One should note that *Boccippio et al.* [2000] calculated the source distribution (%) using source densities, while Buechler calculated the distribution from

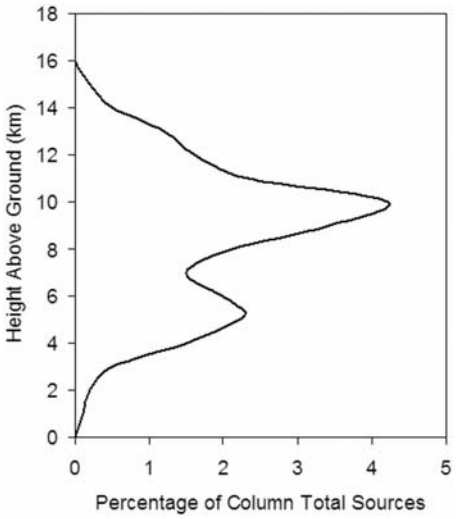

Figure 2. Vertical distribution of mean VHF source frequencies from the North Alabama lightning mapping array (LMA) for three warm seasons (April 2003 to September 2005). The sources were averaged within a 50 km radius of the LMA network and analyzed at a vertical resolution of 0.25 km (after Buechler (personal communication, 2009)).

individual sources, thereby, accounting for the different values on the *x* axes of Figures 1 and 2.

[19] Figure 3 shows our vertical distribution of source percentage (solid line) for all VHF sources within the northern 50 km radius of the KSC LDAR during June, July, and August 2004 and 2005. Only storms that crossed into the 50 km radius were included. Storms that occurred outside or along the edge of the 50 km radius were excluded even if they produced lightning. One should recall that the Melbourne radar is located ~50 km south of LDAR's central receiver. Thus, our selection criteria ensure that (1) virtually all lightning sources will be detected and (2) that a storm will not be so close to the radar that its top cannot be accurately determined.

[20] Our warm season vertical distribution of LDAR sources at KSC (Figure 3) generally is similar to the annual distribution by *Boccippio et al.* [2000] (Figure 1). However, our summer distribution has a broad peak between ~6 and 8 km, while the annual distribution (Figure 1) has a sharper peak at a slightly higher altitude (~9.5 km). The higher altitude annual peak may be due to stronger, higher storms that are associated with middle latitude systems that mostly occur during the cooler months. Florida storms that occur between June and August mostly are triggered by the sea breeze and may not have such high tops.

[21] Although both our summer KSC distribution of source fraction (Figure 3) and Buechler's northern Alabama warm season distribution (Figure 2) exhibit maxima in the middle and upper troposphere, several differences also are evident. The dominant peak in Buechler's distribution is at 9 km, while it occurs between ~6 and 8 km in our distribution. The North Alabama distribution also exhibits a secondary maximum at approximately 5 km that is not contained in either our distribution or that of *Boccippio et al.* [2000].

[22] There are several possible explanations for the differences in Figures 1–3. First, different seasons and detectors were used. *Boccippio et al.* [2000] considered all months, while we considered June–August, both using KSC LDAR data. Buechler (personal communication, 2009) also considered the warm season (April 2003 to September 2005) but employed LMA in northern Alabama. Second, storm structure may differ somewhat between the two locations, even if the same months had been considered. However, it is doubtful that differences between environment and convection at low levels between Florida and northern Alabama totally explain the difference in the vertical distribution of VHF sources near 5 km. Instead, the major issue probably is that results from the newer, more sensitive research quality LMA sensors in northern Alabama are being compared with those from the older, operational LDAR network at KSC. The North Alabama LMA network has 12 receivers, while the KSC network only has 6 sites, and the algorithms used to process the LMA and LDAR data also differ [*Rison et al.*, 1999 versus *Lennon*, 1975]. VHF networks have been shown to preferentially detect negative leaders [*Shao and Krehbiel*, 1996; *Rison et al.*, 1999] because they radiate greater power [*Thomas et al.*, 2001]. This makes it more difficult to assess regions of negative charge [*Rust et al.*, 2005; *Wiens et al.*, 2005; *Wiens*, 2006; *Bruning et al.*, 2007]. The VHF sources in the lower level positive charge center that are routinely measured by the LMA, but not as well detected by LDAR, have smaller source power than the sources associated with the more ubiquitous upper level positive charge center that both networks detect. Therefore, the less sensitive LDAR network does not "see" the relatively low-power sources associated with the lower level positive charge center as well as the LMA system.

[23] The sources comprising negative leaders should be proportional to channel length, but this may not be true for

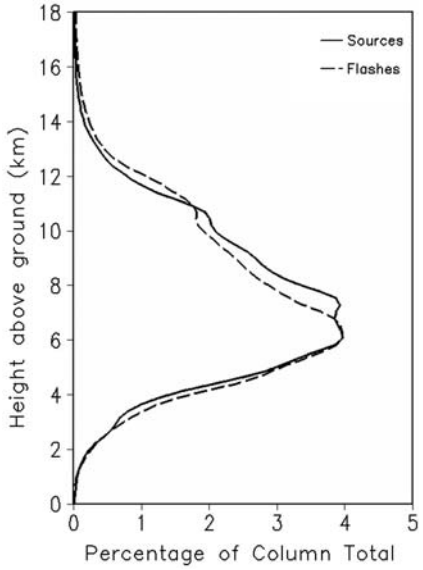

Figure 3. Vertical distribution of warm season average KSC VHF sources (solid line) and flash segments (dashed line) for storms occurring during June, July, and August of 2004 and 2005. Values at a vertical resolution of 0.25 km are expressed as a percentage of the column total.

Table 1. Standard Deviations of VHF Source Fractions (Flash Segments) of the KSC Seasonal Average for All Storms at the Selected Levels[a]

Height (km)	SD (%)
13	0.7 (0.3)
10	2.7 (0.6)
8	3.6 (1.7)
5	2.1 (0.7)

[a]Selected levels are at 5, 8, 10, and 13 km AGL.

positive leaders because they are under sampled (E. Bruning, personal communication, 2009). Therefore, it is important to know whether most of the VHF sources detected by the LDAR are positive or negative. More research will be needed to determine if this is a source of error in the source profiles presented here. However, we hypothesize that our source profiles do not have large errors since over many storms the altitudes of positive charge might vary sufficiently to average out and produce a similar single-peak distribution. This issue currently is being investigated by *Koshak et al.* [2009] and *Peterson and Koshak* [2009].

[24] Included in Figure 3 is the KSC summer season flash segment distribution (dashed line). Flashes were calculated from the source data as described in section 2.3. We counted each segment of each flash in creating Figure 3. For example, if one segment of a flash extended from 4 to 10 km in the vertical, it was counted in each 0.25 km layer between those altitudes. If another segment of the same flash extended from 4 to 9 km, each layer between those altitudes was incremented again. This continued until all segments of a flash were counted at their specific layers. Then, the process began again with segment one of the second flash, and so on. The objective was to include all segments of flashes discharged by the storm. Figure 3 shows little difference between the distributions of source and flash segments. The peak of the flash segment distribution is more narrow, but both occur near the same altitude. Both distributions exhibit a small secondary peak near 11 km AGL. Standard deviations for selected levels of our KSC distributions (Figure 3) are given in Table 1. The sources show a spread of ~1%–4% at the different levels, most likely because the storms included in the distribution have different intensities and are sampled at various stages of their life cycles. However, the standard deviations of flash segments (in parentheses) are smaller than those of sources.

[25] One of the most important characteristics of lightning is its great variability in all four dimensions [e.g., *Koshak et al.*, 2009]. We next strive to describe the vertical variability based on the findings of *Futyan and Del Genio* [2007]. Specifically, we hypothesize that the vertical distribution of lightning varies depending on the height of the echo top above the freezing level. We prepared average vertical profiles of lightning sources (Figure 4a) and flash segments (Figure 4b) for echo tops at 1 km intervals above the assumed 4.5 km freezing level (i.e., at 1, 2, 3 km, and so on above freezing level). Each echo top category included storms with tops within a ~1 km layer. For example, echoes with tops greater than the freezing level but less than or equal to 1 km above the freezing level were included in the layer for 1 km above the freezing level; tops greater than

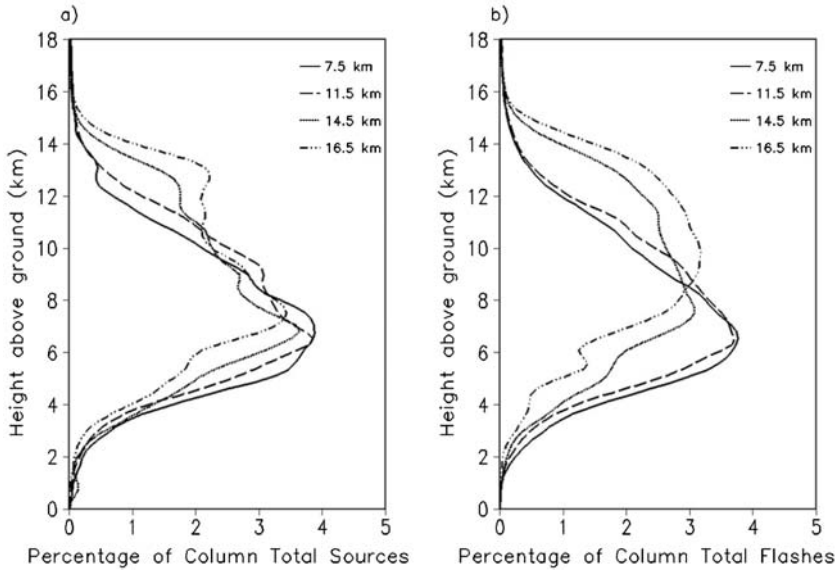

Figure 4. (a). Vertical distributions of VHF source percentages for storms with different radar-derived tops. The solid line represents the source distribution for storms having a radar-derived top 7.5 km AGL (3 km above the freezing level), the dashed line shows the source distribution for storms with tops 11.5 km AGL (7 km above the freezing level), the short dashed line represents storms having tops 14.5 km AGL (10 km above the freezing level), and the dotted line is for storms with tops 16.5 km AGL (12 km above the freezing level). (b) As in Figure 4a but showing the vertical distributions of flash segment percentages for storms with different radar-derived tops. All values were calculated within vertical layers of 0.25 km depth.

1 km above the freezing level but less than or equal to 2 km above the freezing level were included in the profiles for 2 km, and so on.

[26] The methodology used to create the vertical distribution of flash segments in Figure 3 also was used in creating Figure 4b, except that the segments now also are categorized by storm top. Echo top was calculated (as described in section 2.2) based on the maximum height of the 18.5 dBZ radar reflectivity value during each 6 min radar scan at each 1 × 1 km grid point. Thus, the top does not represent the entire storm but the top of each 1 × 1 km grid area. Then, during each volume scan, all sources and flash segments occurring in each echo top height category were averaged over the portion of the domain that contained at least one source/flash segment and finally averaged over the entire multimonth period to create the profiles in Figures 4a and 4b. For ease of presentation, we only present the vertical distributions for storm tops at 7.5, 11.5, 14.5, and 16.5 km AGL (3, 7, 10, and 12 km, respectively, above the assumed 4.5 km freezing level).

[27] The vertical distributions of sources (Figure 4a) and flash segments (Figure 4b) exhibit both similarities and differences. Differences between the four source profiles are smaller than those for flash segments. The major difference is for echo tops at 14.5 and 16.5 km AGL (dot and dash-dot lines, respectively) where the flash segment profiles exhibit broader and higher altitude maxima than do those for sources. Specifically, echo tops of 14.5 km (22,368 sources) and 16.5 km (10,530 sources) AGL exhibit a bimodal source distribution (Figure 4a) with the major peak at ~7 km and a secondary peak between 12 and 14 km. However, the corresponding vertical distributions of flash segments (based on 591 and 118 segments), respectively (Figure 4b) exhibit broad maxima that peak near 7.5 km for tops reaching 14.5 km AGL and near10 km for tops reaching 16.5 km AGL. Considering lower top echoes, the distributions of sources and flash segments for tops at 7.5 km AGL (solid lines) both exhibit a single broad peak at a lower altitude near 7 km AGL, based on 36,287 sources and 317 flash segments. And, echo tops less than 11.5 km AGL display a similar dominant peak near 7 km AGL for both sources and flash segments (based on 99,838 sources and 390 segments). One should note that some sources are above the storm top for these shallower storms. However, since we used the radar-derived storm top threshold of 18.5 km, portions of the cloud and its sources/flash segments are higher than indicated by this threshold. This is evident in the case studies that follow (Figures 5–8). Anvil lightning is an example of this situation. Uncertainty in the data and processing algorithms also cannot be discounted.

[28] We performed a χ^2 test [*Wilks*, 2006] on the vertical distributions of both sources and flash segments to determine if they were significantly different from each other. Visual inspection suggests that the flash profiles for echo tops at 7.5 and 16.5 km are most different. However, the χ^2 value for these profiles is 31.25, compared to 90.53 when assuming 71 degrees of freedom (18 km maximum height at 0.25 km intervals minus one [*Wilks*, 2006]). Therefore, we cannot exclude the null hypothesis that the profiles are from the same distribution. However, this inability does not prove the null hypothesis. Comparisons between other pairs of both sources and flash segments exhibit even smaller calculated values of χ^2.

[29] Standard deviations of sources for each height category are shown in Table 2. These values are smaller than those of all echo tops combined (Table 1), indicating that echo top above freezing level is a factor in explaining the variability in the composite distribution. The standard deviations for flash segments (parentheses, Table 2) are considerably smaller than those for sources. Nonetheless, considerable variation remains. This is examined in the following section.

3.2. Case Studies

[30] We chose four storm days to explore the variability seen in Figure 4b and Table 2. Storms occurring on 2 June, 7 July, 21 August 2004, and 3 August 2005 were selected based on their varying flash densities, average storm tops, and maximum reflectivities (Table 3). One should note that each day's activity did not consist of a single cell that remained within the study domain during its entire life cycle. Instead, a cluster of cells generally formed and/or passed through the domain, with each cell possibly at a different stage of its life cycle. Thus, we cannot relate flash segments to the life cycles of specific cells. The storm tops that are described represent the average top of all grid cells containing precipitation within the domain at each volume scan, not the highest top of the overall storm area at the particular time. We believe this average value better represents what a regional scale numerical model (10–12 km horizontal resolution) would depict. The descriptions that follow indicate large variations between the four storm cases and during the life cycle of each particular case. In general, however, the time of the maximum reflectivity coincides with the time of maximum flash density, with both occurring shortly after the maximum echo top is reached.

[31] The storm activity on 2 June 2004 was associated with a strong middle latitude system and developed in a region of strong vertical wind shear. The morning KSC sounding indicates a convective available potential energy (CAPE) of 1107 J kg^{-1}. This storm day exhibits the weakest peak flash density of the four cases (0.15 km^{-3}, Table 3). The multicellular storm forms (~1900 UTC) and decays (~2200 UTC) within our domain. A secondary cluster of storms forms at ~2000 UTC and merges with the initial cluster. It is at this time that the maximum echo height (13.5 km AGL) occurs, coinciding with the peak flash density (Figure 5a and Table 3). The initial flash density maximum (values greater than 0.14 flash segments km^{-3}) occurs at ~6 km AGL, and by 2040 UTC, a second maximum appears between 6 and 9 km (Figure 5a). At the time of peak flash density (2000 UTC), the maximum reflectivity (46 dBZ) occurs at a height of ~4 km. Then, as the large cluster of storms decays at ~2100 UTC, storm height decreases and the maximum flash density decreases in magnitude and slopes downward with time. By 2200 UTC, a portion of the very weak cluster of thunderstorms is partially outside our domain.

[32] We were especially interested in the percentage of flash segments occurring at each level (Figure 5b). Its vertical distribution and temporal variability are quite different from those of flash segment density (Figure 5a). As the storm intensifies and merges with the secondary cluster at

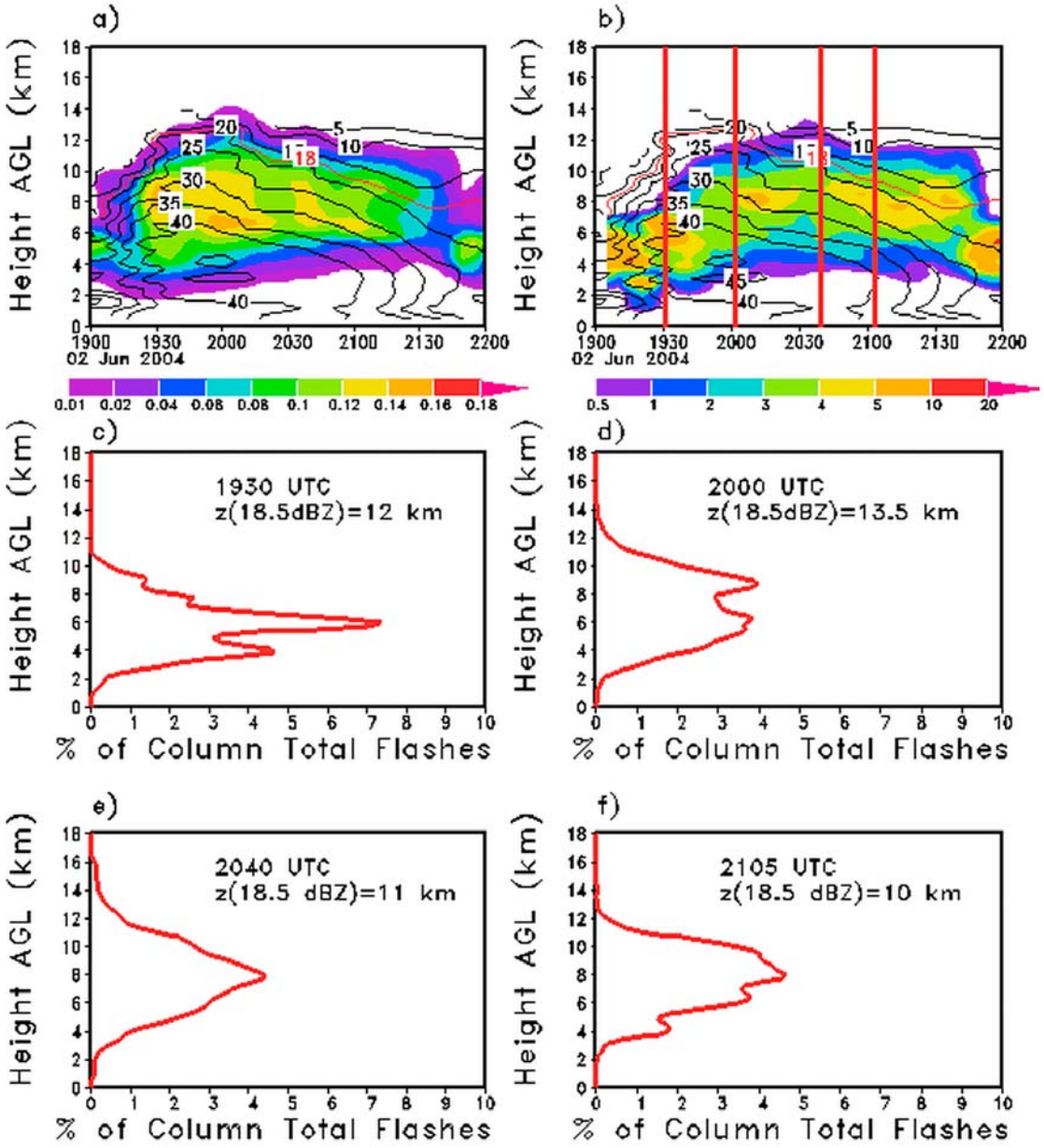

Figure 5. Time series of flash distributions for a storm occurring on 2 June 2004 between 1900 and 2200 UTC near KSC. (a) Colored areas are LDAR-derived flash density (flash segments km^{-3}) computed within the northern 50 km radius of the LDAR central receiver, and contours are area-averaged KMLB radar reflectivity (dBZ), with the 18.5 dBZ contour in red to indicate storm top height. (b) Colored areas are LDAR derived flash segment percentages (% of column total) where the thick vertical red lines correspond to Figures 5c, 5d, 5e, and 5f, respectively. Contours are area-averaged KMLB radar reflectivity with the 18.5 dBZ contour in red to indicate storm top height. (c) Vertical distribution of flash segments (%) at 1930 UTC. (d) Vertical distribution of flash segments (%) at 2000 UTC. (e) Vertical distribution of flash segments (%) at 2040 UTC. (f) Vertical flash segment distribution (%) at 2105 UTC. Values are given at vertical intervals of 0.25 km.

~2000 UTC, the altitude of maximum flash segment percentage slopes upward with time and then slopes downward as the storm dissipates. When the average storm top is less than ~9 km, the majority of flash segments are between 4 and 8 km. However, as the average storm top becomes higher (greater than 9 km) and flash density starts to increase (Figure 5a), most flash segments are distributed between 4 and 14 km.

[33] The four vertical red lines in Figure 5b denote times of the vertical cross sections of flash segment percentage in Figures 5c–5f. Figure 5c depicts the distribution at 1930 UTC when the average storm top is ~12 km. The cross section shows a narrow distribution, with a primary peak near 6 km

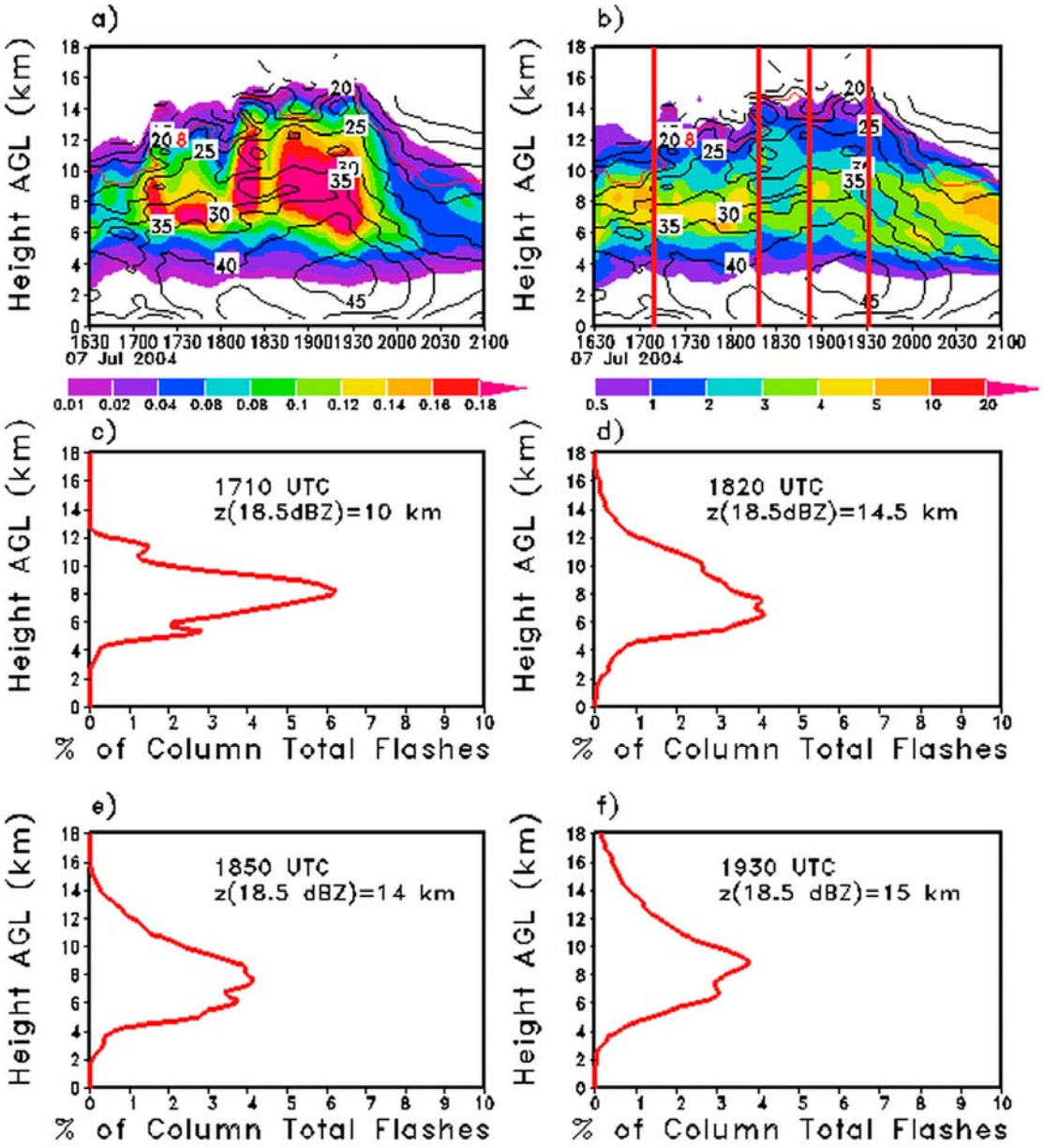

Figure 6. (a and b) As in Figure 5 but for a storm occurring on 7 July 2004 between 1630 and 2100 UTC near KSC. (c) Vertical distribution of flash segments (%) at 1710 UTC. (d) Vertical distribution of flash segments (%) at 1820 UTC. (e) Vertical distribution of flash segments (%) at 1850 UTC. (f) Vertical flash segment distribution (%) at 1930 UTC.

and a secondary peak near 4 km. The vertical distribution at 2000 UTC when the average storm top is highest (13.5 km, Figure 5d) is bimodal with peaks near 5.5 and 9 km. This time corresponds to the increase in flash density in Figure 5a. When the flash density begins to increase a second time at ~2040 UTC (Figure 5e), the average storm top is ~11 km, and most flash segments are between 4 and 14 km with a maximum near 8 km. Finally, as the peak flash density decreases in magnitude at ~2105 UTC (Figure 5f), the greatest percentage of flash segments is between 7 and 10 km, with two minor peaks at lower altitudes.

[34] The 7 July 2004 storm area, with a peak flash segment density of 0.18 km^{-3} occurs in a weak wind shear environment with speeds less than 2.5 m s^{-1} up to 200 hPa and a CAPE of 2868 J kg^{-1}. Convection on this day and the two cases that follow were initiated by the sea breeze. This storm day has the highest average echo top (15 km, Table 3) of the four cases and exhibits several pulses of enhanced flash segment density (Figure 6a). The multicell storm begins with five small cells oriented in a north to south direction across the center of our domain. As the cells mature and move offshore, they remain in our domain until they decay at ~1900 UTC. Then, at ~1830 UTC, a large cluster of storms moves into our domain from the west, coinciding with an initial pulse of enhanced flash density (Figure 6a). As the storm grows between 1800 and 1930

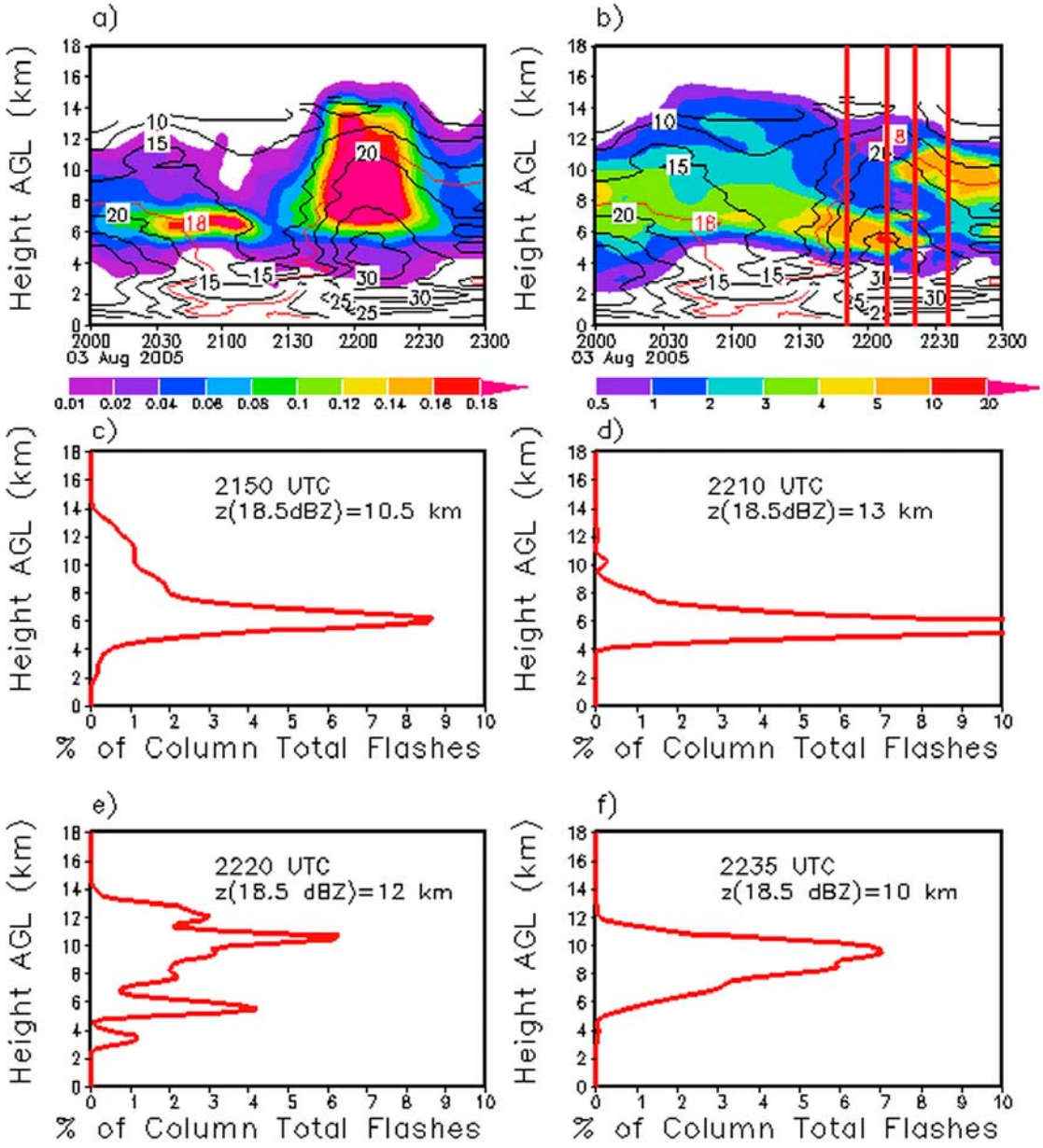

Figure 7. (a and b) As in Figure 5 but for a storm occurring on 3 August 2005 from 2000 UTC to 2300 UTC near KSC. (c) Vertical distribution of flash segments (%) at 2150 UTC. (d) Vertical distribution of flash segments (%) at 2210 UTC. (e) Vertical distribution of flash segments (%) at 2220 UTC. (f) Vertical flash segment distribution (%) at 2235 UTC.

UTC, maximum flash density is between 6 and 12 km. The average storm top increases to 15 km at 1820 UTC, and the flash density exceeds 0.18 km^{-3} between ~1845 and 1930 UTC when the average storm top is near 15 km. The large cluster of storms fills a major portion of our domain as it merges with another weak cell that forms within our domain near 1930 UTC. This merger could explain why the average storm top increases slightly from 1900 to 1930 UTC and why there is another pulse of enhanced flash density (Figure 6a). As in the 2 July storm, maximum reflectivity (46 dBZ) occurs at ~3.75 km, corresponding to the approximate time (1925 UTC) of maximum flash density (0.18 km^{-3}). Then, as average storm height decreases from ~1900 to 2000 UTC, maximum flash density decreases and slopes downward with time as observed on 2 June. The exception is the pulse at ~1930 UTC.

[35] The pulsing of flash segment density (Figure 6a) is associated with changes in the vertical distribution of the flash segments (Figures 6b–6f). As the storm grows taller, the percentage of segments in the upper levels increases (Figure 6b). The flash segment density begins to increase at ~1710 UTC when the average storm top is ~10 km. Most flash segments at this time are located between 6 and 10 km (Figure 6c). Corresponding to the first peak in average

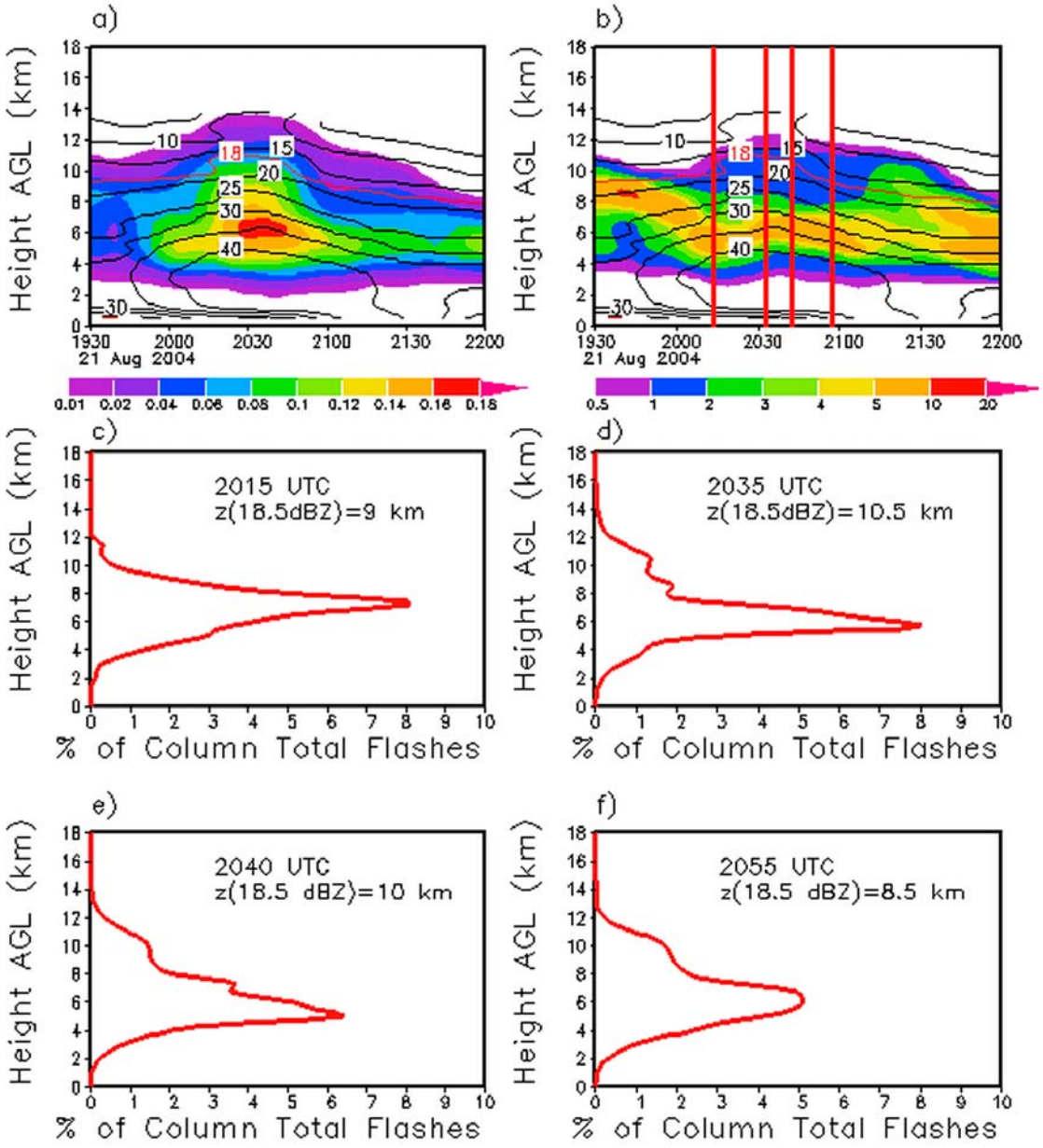

Figure 8. (a and b) As in Figure 5 but for a storm occurring on 21 August 2004 from 1930 UTC to 2200 UTC near KSC, Fla. (c) Vertical distribution of flash segments (%) at 2015 UTC. (d) Vertical distribution of flash segments (%) at 2035 UTC. (e) Vertical distribution of flash segments (%) at 2040 UTC. (f) Vertical flash segment distribution (%) at 2055 UTC.

storm top and the first pulse of enhanced flash density at ~1820 UTC (Figure 6d), the percentage distribution broadens and lowers. However, when the second maximum in flash density occurs and the average storm top decreases at ~1850 UTC, the flash distribution again narrows (Figure 6e), with the greatest values between 7 and 10 km. Finally, during the last pulse in flash density when the average storm top increases slightly at ~1930 UTC (Figure 6f), the vertical profile again broadens.

[36] The 3 August 2005 sea breeze-induced storm area also occurs in a weak wind shear environment with winds aloft less than 7.5 m s^{-1} and a CAPE of 3475 J kg^{-1}. This

Table 2. Standard Deviations of VHF Source Fractions (Flash Segment Fractions) for Storm Top Heights for the Selected Levels[a]

Height (km)	SD (%) 16.5 km AGL	SD (%) 14.5 km AGL	SD (%) 11.5 km AGL	SD (%) 7.5 km AGL
13	0.4 (0.08)	0.5 (0.1)	0.8 (0.2)	0.7 (0.3)
10	1.2 (0.08)	1.7 (0.3)	1.9 (0.5)	2.3 (0.5)
8	1.5 (0.08)	2.4 (0.2)	2.5 (0.6)	2.9 (0.5)
5	0.9 (0.08)	1.1 (0.1)	1.5 (0.5)	2.1 (0.6)

[a]Storm top heights are at 7.5, 11.5, 14.5, and 16.5 km AGL (corresponding to Figure 4 legend) for the selected levels of 5, 8, 10, and 13 km AGL.

Table 3. Storm Parameters for Case Studies on 2 June, 7 July, and 21 August 2004 and on 3 August 2005[a]

Storm Parameter	2 June 2004	7 July 2004	3 August 2005	21 August 2004
Maximum storm top	13.5 km	15 km	13 km	10.5 km
Maximum flash density	0.15 km^{-3}	0.18 km^{-3}	0.22 km^{-3}	0.17 km^{-3}
Height of maximum flash density	6 km`	10 km	9 km	6 km
Maximum flash %	8%	11%	19%	12%
Height of maximum flash %	8 km	7 km	6 km	8 km
Maximum reflectivity	46 dBZ	46 dBZ	43 dBZ	46 dBZ
Height of maximum reflectivity	4.00 km	3.75 km	4.75 km	2.50 km

[a]Heights are in AGL.

storm has the greatest flash segment density (0.22 km^{-3}) of our examples and a maximum average top of 13 km (Table 3). Two cells form ~90 km northwest of the radar at ~2015 UTC. This small cluster moves outside of our domain by 2130 UTC before it decays. At approximately the same time, a large multicellular storm enters the domain. The maximum average height occurs at ~2210 UTC as flash segment density reaches a maximum between 6 and 14 km (Figure 7a). As in the previous two cases, the time of maximum reflectivity (43 dBZ at ~4.75 km) corresponds to the time of greatest flash density located near 6 km. The flash density then decreases as the storm dissipates. The vertical distributions of percentage flash segments (Figure 7b) again are quite different from those of flash density (Figure 7a). For example, at the time of the deep layer of flash density (2200 UTC), the layer of large percentages is much thinner. The vertical distributions in Figures 7c and 7d correspond to the beginning and end, respectively, of the small upward bulge in flash density between ~2150 and 2210 UTC (Figure 7a). At the beginning of the bulge, the greatest percentage is near 6 km, with a weak secondary maximum between 10 and 14 km. However, at the end of the vertical protrusion, the secondary peak has virtually disappeared, although the primary peak is much stronger and remains at 6 km. Figures 7e (2220 UTC) and 7f (2235 UTC) show that the greatest percentages of flash segments now are located at much higher altitudes. The difference between profiles of source density (Figure 7a) and percentage flash segments (Figure 7b) is striking at ~2235 UTC. An examination of radar data at this time indicates that the storm area has virtually dissipated within our domain, with few sources or flash segments. However, those that do occur are located in the anvil region of the storm.

[37] The storms on 21 August 2004 exhibit the lowest average echo top of the cases presented (10.5 km, Table 3), but exhibit a moderately strong maximum flash segment density of 0.17 km^{-3}. The environmental winds reach 17 m s^{-1}, and the CAPE is 3664 J kg^{-1}. The storms on this day form at ~1945 UTC as two small cells between 50 and 75 km northwest of the radar. This initial weak cluster of storms merges with two additional cells that enter the domain from the south at ~2015 UTC. Shortly thereafter (at ~2030 UTC), the storm area exhibits a maximum flash density near 6 km (Figure 8a) when the average storm top reaches its peak altitude of ~10.5 km. Maximum reflectivity (46 dBZ) at ~2.5 km again corresponds to the storm's peak flash density (at 6 km). The cluster of storms stays within the domain and begin to weaken, corresponding to a decrease in average storm height from ~2045 to 2145 UTC, and maximum flash segment density (exceeding 0.14 km^{-3}) decreasing and sloping downward. Figure 8b shows the vertical distribution of flash percentage, where the vertical red lines correspond to Figures 8c–8f. The altitudes of greatest percentage show relatively little variation after ~2015 UTC. The distribution of source percentage at ~2015 UTC (Figure 8c), just as the storm begins to grow and intensify, exhibits a sharp peak near 8 km. Figures 8d and 8e correspond to 2035 and 2040 UTC when the average storm top is highest and flash density is greatest. During these times, the greatest percentage of flash segments lowers to near 6 km. Finally, the greatest number of segments at 2055 UTC (Figure 8f) occurs at 6 km, with a secondary peak near 10 km.

4. Discussion and Conclusions

[38] Relatively few studies have investigated climatological and storm-to-storm variations in lightning distributions. And, to our knowledge, none have considered how source and flash percentage vary through time. Our vertical profile of lightning sources for KSC's entire warm season compares well with that of *Boccippio et al.* [2000] and has many similarities to the North Alabama warm season storms of Buechler (personal communication, 2009). The differences that are observed can be attributed to the different sensors and processing algorithms that are used, and to the different seasons and storm characteristics that occur. The vertical distribution of sources (Figure 3) exhibits a large standard deviation at each altitude (Table 1). When we categorized the sources by their height above the freezing level (Figure 4a), the profiles exhibit a smaller standard deviation (Table 2). These results suggest that storm top above freezing level is a useful parameter for vertically distributing lightning sources. Nonetheless, the standard deviations still indicate that the profiles exhibit large variability.

[39] Previous case studies of total lightning observations have focused on severe storms [e.g., *Carey et al.*, 2005; *Hodapp et al.*, 2008; *Ely et al.*, 2008; *Thomas et al.*, 2000; *Krehbiel et al.*, 2000; *Rison et al.*, 1999]. Even though the composite results presented here included storms of all intensities, their source density and vertical structure have similarities to the severe storms. Studies of leading line trailing stratiform MCSs in Texas showed that the majority of VHF lightning sources were in the leading convective line and exhibited a vertically bimodal pattern [*Carey et al.*, 2005; *Hodapp et al.*, 2008; *Ely et al.*, 2008]. Source densities for our composite thunderstorms over Florida also exhibit a bimodal pattern, especially for the highest top storms (Figure 4a). A conceptual model of severe thunder-

storm charge structure by *Dotzek et al.* [2005] showed that negative charge regions typically occur between −10°C and −20°C, whereas the positive charge region typically occurs near the −40°C level. Although their study considered severe storms, once again, there are similarities with our mostly nonsevere cases.

[40] We then combined our sources into flash segments and examined the vertical distribution of flash segment percentages (Figures 3 and 4b). The vertical distributions of sources (Figure 4a) and flash segments (Figure 4b) exhibit some similarities. The major difference is for echo tops at 14.5 and 16.5 km AGL where the profiles for flash segments exhibit broader and higher altitude maxima than do those for sources. Specifically, echo tops of 14.5 km and 16.5 km AGL exhibit a bimodal source distribution (Figure 4a) with the major peak at ~7 km and a secondary peak between 12 and14 km. However, the corresponding vertical distributions of flash segments (Figure 4b) exhibit broad maxima that peak near 7.5 km for tops reaching 14.5 km AGL and near10 km for tops reaching 16.5 km AGL. The distributions of sources and flash segments for tops at 7.5 km and 11.5 km AGL both exhibit a single broad peak near 7 km AGL. We performed a χ^2 test [*Wilks*, 2006] on the vertical distributions of sources and flash segments to determine if they were significantly different from each other. In all pairings we could not exclude the null hypothesis that the profiles were from the same distribution.

[41] The vertical profiles of flash segment percentages in the four case studies generally are quite different from those of the sources. The flash percentages show considerable temporal variability (Figures 5c–5d to 8c–8d), with the height of the flash maximum varying over a broad layer between 6 and 10 km AGL (Table 3). Nonetheless, the results demonstrate a general relation between radar-derived storm top and flash percentage distributions in warm season Florida thunderstorms. Storms with relatively low tops and weak intensity generally tend to exhibit a single dominant peak in the percentage profile, while those with higher tops (greater than 10 km AGL) and stronger intensity generally exhibit multiple peaks of percentage. However, the four case studies demonstrate that the flash percentage profiles vary considerably, most likely due to differences in storm structure and the stage of their life cycles.

[42] Several factors help explain the observed large variability in the vertical profiles. Many vertical charge profiles have been documented in active convection, including dipoles, inverted dipoles, and tripoles [e.g., *Carey et al.*, 2005; *Lang and Rutledge*, 2008; *MacGorman et al.*, 2005; *Mo et al.*, 2002]. And, as many as six charge layers are common in the stratiform regions of MCSs [*Stolzenburg et al.*, 1998]. The charging mechanisms within storms are related to the vertical profiles of hydrometeors [e.g., *Rutledge et al.*, 1992; *Carey and Rutledge*, 1996; *Petersen et al.*, 1996, 1999, 2005; *Deierling et al.*, 2005, 2008; *Kuhlman et al.*, 2006] that are influenced by the strength of the storm's updraft and the vertical temperature distribution. These factors determine the charge distribution and whether flashes will be positive or negative, IC or CG, have strong or weak peak currents, and are frequent or sparse. Furthermore, *Bluestein and MacGorman* [1998] showed that the relation between the genesis of severe events and the polarity and cloud-to-ground flash rates even varies widely in nearby storms on the same day.

[43] Much remains to be learned about the storm-to-storm variability of hydrometeor profiles and their relation to charging and lightning characteristics. For example, it would be useful to analyze the life cycle of a large sample of convective cells to generalize their results regarding temporal evolution of lightning with height. As additional diagnostic studies are made, the findings can be incorporated into sophisticated lightning parameterization modules for chemical transport models. This effort already has begun for cloud resolving models [e.g., *Deierling et al.*, 2005; *Barthe and Pinty*, 2007]. Furthermore, *Koshak et al.* [2009] relate NO production to the number of 1 m flash channel lengths, with initial results described in the study of *Peterson and Koshak* [2009].

[44] We hypothesize that the distributions presented in Figure 4b are appropriate as a first step toward parameterizing lightning-produced NOx in regional scale models of Florida and perhaps the southeast United States. However, more research will be needed to determine if these distributions are appropriate for other seasons and in other areas of the world. The studies of geographic variability will be hampered by the small number of LMA sites. We currently are incorporating the current distributions into a lightning NOx parameterization scheme for use in the Weather Research and Forecasting-Chemistry model when run on a regional scale. Those results will be presented in a future paper.

[45] **Acknowledgments.** This research was supported in part by NASA's Global Tropospheric Chemistry Program through grant NNX08AH72G to Florida State University. We appreciate the assistance of Dennis Buechler and Geoffrey Stano at NASA's Marshall Space Flight Center who answered many questions about source distributions in northern Alabama and Kennedy Space Center, Fla. We also thank Robert Hart and Scott Rudlosky at The Florida State University for their technological assistance, and Eric Bruning at the University of Maryland for his technical advice and expertise. Jon Ahlquist at Florida State assisted with the statistical analyses. Finally, three anonymous reviewers provided valuable suggestions that improved the manuscript.

References

Amburn, S. A., and P. L. Wolf (1997), VIL density as a hail indicator, *Weather Forecasting*, *12*, 473–478.

Barthe, C., and M. C. Barth (2008), Evaluation of a new lightning-produced NO_x parameterization for cloud resolving models and its associated uncertainties, *Atmos. Chem. Phys.*, *8*, 4691–4710.

Barthe, C., and J.-P. Pinty (2007), Simulation of a supercellular storm using a three-dimensional mesoscale model with an explicit lightning flash scheme, *J. Geophys. Res.*, *112*, D06210, doi:10.1029/2006JD007484.

Barthe, C., J. P. Pinty, and C. Mari (2007), Lightning-produced NOx in an explicit electrical scheme tested in a stratosphere-troposphere experiment: Radiation, aerosols, and ozone case study, *J. Geophys. Res.*, *112*, D04302, doi:10.1029/2006JD007402.

Bluestein, H. B., and D. R. MacGorman (1998), Evolution of cloud-to-ground lightning characteristics and storm structure in the Spearman, Texas, tornadic supercells of 31 May 1990, *Mon. Weather Rev.*, *126*, 1451–1467.

Boccippio, D. J., S. Heckman, and S. J. Goodman (2000), A diagnostic analysis of the Kennedy Space Center LDAR network 1. Data characteristics, *J. Geophys. Res.*, *106*, 4769–4786, doi:10.1029/2000JD900687.

Britt, T. O., C. L. Lenon, and L. M. Maier (1998), *Lightning Detection and Ranging System*, NASA Tech Brief, *22*(4), 60–61.

Bruning, E. C., W. D. Rust, T. J. Schuur, D. R. MacGorman, P. R. Krehbeil, and W. Rison (2007), Electrical and polarimetric radar observations of a multicell storm in TELEX, *Mon. Weather Rev.*, *135*, 2525–2544.

Carey, L. D., and S. A. Rutledge (1996), A multiparameter radar case study of the microphysical and kinematic evolution of a lightning producing storm, *J. Meteorol. Atmos. Phys.*, *59*, 33–64.

Carey, L. D., M. J. Murphy, T. L. McCormick, and N. W. S. Dermetriades (2005), Lightning location relative to storm structure in a leading-line, trailing-stratiform mesoscale convective system, *J. Geophys. Res.*, *110*, D03105, doi:10.1029/2003JD004371.

Crum, T. D., and R. L. Alberty (1993), The WSR-88D and the WSR-88D operation support facility, *Bull. Am. Meteorol. Soc.*, *74*, 1669–1668.

Curran, E. B., R. L. Holle, and R. E. Lopez (2000), Lightning casualties and damages in the United States from 1959–1994, *J. Clim.*, *13*, 3448–3464.

DeCaria, A. J., K. E. Pickering, G. L. Stenchikov, and L. E. Ott (2005), Lightning-generated NO_x and its impact on tropospheric ozone production: A three-dimensional modeling study of a Stratosphere-Troposphere Experiment: Radiation, Aerosols, and Ozone (STERAO-A) thunderstorm, *J. Geophys. Res.*, *110*, D14303, doi:10.1029/2004JD005556.

Deierling, W., J. Latham, W. A. Petersen, S. M. Ellis, and J. H. J. Christian (2005), On the relationship of thunderstorm ice hydrometeor characteristics and total lightning measurements, *Atmos. Res.*, *76*, 114–126.

Deierling, W., W. A. Petersen, J. Latham, S. Ellis, and H. J. Christian (2008), The relationship between lightning activity and ice fluxes in thunderstorms, *J. Geophys. Res.*, *113*, D15210, doi:10.1029/2007JD009700.

Dotzek, N., R. M. Rabin, L. D. Carey, D. R. MacGorman, T. L. McCormaic, N. W. Demetriades, M. J. Murphy, and R. L. Holle (2005), Lightning activity related to satellite and radar observations of a mesoscale convective system over Texas on 7–8 April 2002, *Atmos. Res.*, *76*, 127–166.

Ely, B. L., R. E. Orville, L. D. Carey, and C. L. Hodapp (2008), Evolution of total lightning structure in a leading line trailing stratiform mesoscale system over Houston, Texas, *J. Geophys. Res.*, *113*, D08114, doi:10.1029/2007JD008445.

Futyan, J. M., and A. D. Del Genio (2007), Relationships between lightning and properties of convective cloud clusters, *Geophys. Res. Lett.*, *34*, L15705, doi:10.1029/2007GL030227.

Goodman, S. J., et al. (2005), The North Alabama lightning mapping array: Recent severe storm observations and future prospects, *Atmos. Res.*, *76*, 423–437.

Hodapp, C. L., L. D. Carey, and R. E. Orville (2008), Evolution of radar reflectivity and total lightning characteristics of the 21 April 2006 mesoscale convective system over Texas, *Atmos. Res.*, *89*, 113–137.

Koshak, W. J., M. N. Khan, A. P. Biazar, M. Newchurch, and R. T. McNider (2009), A NASA model for improving the lightning NOx emission inventory for CMAQ, 4th Conference on Meteorological Applications of Lightning Data, Am. Meteorol. Soc., Phoenix, Ariz, 11–15 January.

Krehbiel, P. R., R. J. Thomas, W. Rison, T. Hamlin, J. Harlin, and M. Davis (2000), GPS-based mapping system reveals lightning inside storms, *Eos, Trans. Am. Geophys. Union*, *81*, 21–25.

Kuhlman, K. M., C. L. Ziegler, E. R. Mansell, D. R. MacGorman, and J. M. Straka (2006), Numerically simulated electrification and lightning of the 29 June 2000 STEPS supercell storm, *Mon. Weather Rev.*, *134*, 2734–2757.

Lakshmanan, V., T. Smith, G. Stumpf, and K. Hondl (2007a), The warning decision support system—integrated information (WDSS-II), *Weather Forecasting*, *22*, 592–608.

Lakshmanan, V., T. Smith, K. Hondl, G. Stumpf, and A. Witt (2007b), An automated technique to quality control radar reflectivity data, *J. Appl. Meteorol.*, *46*, 288–305.

Lang, T. J., and S. A. Rutledge (2008), Kinematic, microphysical and electrical aspects of an asymmetric bow-echo mesoscale convective system observed during STEPS 2000, *J. Geophys. Res.*, *113*, D08213, doi:10.1029/2006JD007709.

Lennon, C. L. (1975), LDAR—A new lightning detection and ranging system, *Eos, Trans. Am. Geophys. Union*, *56*, 991.

Lyons, W. A., E. R. Williams, S. A. Cummer, and M. A. Stanley (2003), Characteristics of sprite-producing positive cloud-to-ground lightning during the 19 July 2000 STEPS mesoscale convective systems, *Mon. Weather Rev.*, *131*, 2417–2427.

MacGorman, D. R., W. D. Rust, P. Krehbiel, W. Rison, E. Bruning, and K. Wiens (2005), The electrical structure of two supercell storms during STEPS, *Mon. Weather Rev.*, *133*, 2583–2607.

McNamara, T. M. (2002), The horizontal extent of cloud-to-ground lightning over Kennedy Space Center, M.S. thesis, Dep. of Eng. Phys, Air Force Institute of Technology, Wright-Patterson AFB, Ohio, 114 pp.

Maier, L., C. Lennon, T. Britt, and S. Schaefer (1995), LDAR system performance and analysis, in *Proceedings of International Conference on Cloud Physics*, Am. Meteorol. Soc., Boston, Mass.

Mansell, E. R., C. L. Ziegler, and E. C. Bruning (2010), Simulated electrification of a small thunderstorm with two-moment bulk microphysics, *J. Atmos. Sci.*, *67*, 171.

Mo, Q., J. H. Helsdon Jr., and W. P. Winn (2002), Aircraft observations of the creation of lower positive charges in thunderstorms, *J. Geophys. Res.*, *107*(D22), 4616, doi:10.1029/2002JD002099.

Murphy, M. J., K. L. Cummins, and L. M. Maier (2000), The analysis and interpretation of three- dimensional lightning flash information, *16th Int. Conf. on IIPS for Meteorol., Oceanogr., Hydrol.*, Am. Meteorol. Soc., Long Beach, Calif., 102–105.

Nelson, L. A. (2002), Synthesis of 3-dimensional lightning data and radar to determine the distance that naturally occurring lightning travels from thunderstorms, M.S. thesis, Air Force Institute of Technology, Wright-Patterson AFB, Ohio, 85 pp.

Orville, R. E. (2008), Development of the National Lightning Detection Network, *Bull. Am. Meteorol. Soc.*, *89*, 180–190.

Ott, L. E., K. E. Pickering, G. L. Stenchikov, H. Huntrieser, and U. Schumann (2007), Effects of lightning NOx production during the 21 July European Lightning Nitrogen Oxides Project storm studied with a three-dimensional cloud-scale chemical transport model, *J. Geophys. Res.*, *112*, D05307, doi:10.1029/2006JD007365.

Ott, L., K. Pickering, G. Stenchikov, D. Allen, A. DeCaria, B. Ridley, R.-F. Lin, S. Lang, and W.-K. Tao (2010), Production of lightning NOx and its vertical distribution calculated from 3-D cloud-scale chemical transport model simulations, *J. Geophys. Res.*, *115*, D04301, doi:10.1029/2009JD011880.

Petersen, W. A., S. A. Rutledge, and R. E. Orville (1996), Cloud-to-ground lightning observations to TOGA COARE. Selected results and lightning location algorithm, *Mon. Weather Rev.*, *124*, 602–620.

Petersen, W. A., S. A. Rutledge, R. C. Cifelli, B. S. Ferrier, and B. F. Smull (1999), Shipborne Dual-Doppler operations during TOGA COARE: Integrated observations of storm kinematics and electrification, *Bull. Am. Meteorol. Soc.*, *80*, 81–96.

Petersen, W. A., H. J. Christian, and S. A. Rutledge (2005), TRMM observations of the global relationship between ice water content and lightning, *Geophys. Res. Lett.*, *32*, L14819, doi:10.1029/2005GL023236.

Peterson, H., and W. Koshak (2009), An algorithm for obtaining the distribution of 1-meter lightning channel segment altitudes for application in lightning NOx production estimation, Fall Meeting, Am. Geophys. Union, 14–18 December 2009.

Poehler, H. A., and C. L. Lennon (1979), Lightning Detection and Ranging (LDAR) System Description & Performance Objectives, NASA Technical Memorandum 74106, 86 pp.

Pickering, K. E., Y. Wang, W. K. Tao, C. Price, and J. F. Muller (1998), Vertical distributions of lightning NOx for use in regional and global chemical transport models, *J. Geophys. Res.*, *103*, 31,203–31,216, doi:10.1029/98JD02651.

Price, C., and D. Rind (1992), A simple lightning parameterization for calculating global lightning distributions, *J. Geophys. Res.*, *97*, 9919–9933, doi:10.1029/92JD00719.

Rison, W., R. J. Thomas, P. R. Hamlin, and J. Harlin (1999), A GPS-based three-dimensional lightning mapping system: Initial observation in central New Mexico, *Geophys. Res. Lett.*, *26*(23), 3573–3576, doi:10.1029/1999GL010856.

Rust, W. D., D. R. MacGorman, E. C. Bruning, S. A. Weiss, P. R. Krehbiel, R. J. Thomas, W. Rison, T. Hamlin, and J. Harlin (2005), Inverted-polarity electrical structures in thunderstorms in the Severe Thunderstorm Electrification and Precipitation Study, *Atmos. Res.*, *76*, 247–271.

Rutledge, S. A., E. R. Williams, and T. D. Keenan (1992), The down under Doppler and electricity experiment (DUNDEE): Overview and preliminary results, *Bull. Am. Meteorol. Soc.*, *73*, 3–16.

Schumann, U., and H. Huntrieser (2007), The global lightning-induced nitrogen oxides source, *Atmos. Chem. Phys.*, *7*, 3823–3907.

Shao, X. M., and P. R. Krehbiel (1996), The spatial and temporal development of intracloud lightning, *J. Geophys. Res.*, *101*(D21), 26,641–26,668, doi:10.1029/96JD01803.

Stocks, B. J., et al. (2002), Large forest fires in Canada, 1959–1997, *J. Geophys. Res.*, *107*, 8149, doi:10.1029/2001JD000484 [printed *108* (D1), 2003].

Stolzenburg, M., W. D. Rust, and T. C. Marshall (1998), Electrical structure in thunderstorm convective regions 2. Isolated storms, *J. Geophys. Res.*, *103*(D12), 14,079–14,096, doi:10.1029/97JD03547.

Thomas, R. J., P. R. Krehbiel, W. Rison, T. Hamlin, D. J. Boccippio, S. J. Goodman, and H. J. Christian (2000), Comparison of ground-based 3-dimensional lightning mapping observations with satellite-based LIS observations in Oklahoma, *Geophys. Res. Lett.*, *27*(12), 1703–1706, doi:10.1029/1999GL010845.

Thomas, R. J., P. R. Krehbiel, W. Rison, T. Hamlin, J. Harlin, and D. Shown (2001), Observations of VHF source powers radiated by lightning, *Geophys. Res. Lett.*, *28*(1), 143–146, doi:10.1029/2000GL011464.

Wiens, K. C. (2006), Thunderstorm electrical structures observed by lightning mapping arrays, *Preprints, 2nd Conf. Meteor. Applications of Lightning Data*, Am. Meteorol. Soc., Atlanta, Ga, CD-ROM, 3.1.

Wiens, K. C., S. A. Rutledge, and S. A. Tessendorf (2005), The 29 June 2000 supercell observed during STEPS. Part II: Lightning and charge structure, *J. Atmos. Sci.*, *62*, 4151–4177.

Wilks, D. S. (2006), *Statistical Methods in the Atmospheric Sciences*, 2nd Ed., International Geophysics Series, Vol. 91, Academic Press, 627 pp.

U.S. Department of Commerce (2006), Doppler radar meteorological observations part c, *Federal Meteorological Handbook 11*, 105 pp.

H. E. Fuelberg and A. E. Hansen, Department of Meteorology, Florida State University, Tallahassee, FL 32306-4520, USA. (fuelberg@met.fsu.edu; ahopkins@met.fsu.edu)

K. E. Pickering, NASA Goddard Space Flight Center, Greenbelt, MD 20771, USA. (kenneth.e.pickering@nasa.gov)